COMPUTATIONAL FLUID DYNAMICS AS A MEANS TO ASSESS THE INFLUENCE OF AERODYNAMIC FORCES ON PANTOGRAPH AVERAGE CONTACT FORCE

Journal:	*Part F: Journal of Rail and Rapid Transit*
Manuscript ID:	JRRT-15-0080
Manuscript Type:	Article
Date Submitted by the Author:	12-May-2015
Complete List of Authors:	Carnevale, Marco; Politecnico di Milano, Dipartimento di Meccanica Facchinetti, Alan; Politecnico di Milano, Dipartimento di Meccanica Maggiori, Luca; Politecnico di Milano, Dipartimento di Meccanica Rocchi, Daniele; Politecnico di Milano, Dipartimento di Meccanica
Keywords:	Pantograph-catenary interaction, Train aerodynamics, Computational Fluid Dynamics, High speed, Pantograph kinematics
Abstract:	This paper discusses the possibility to adopt Computational Fluid Dynamics (CFD) to assess the influence of aerodynamic forces (aerodynamic uplift) on the mean contact force acting between pantograph and contact wire. The analysis is carried out through experimental tests and CFD simulations, performed both in wind tunnel and on-track scenarios. A method for the computation of the aerodynamic uplift and for the assessment of the contact force unbalance between leading and trailing collector is proposed. It is based on the virtual work principle, and exploits both the numerical forces resulting from CFD analysis and the Jacobian terms obtained from pantograph kinematic analysis. The proposed model only takes into account stationary phenomena; it is fully validated by means of experimental results.

COMPUTATIONAL FLUID DYNAMICS AS A MEANS TO ASSESS THE INFLUENCE OF AERODYNAMIC FORCES ON PANTOGRAPH AVERAGE CONTACT FORCE

Marco CARNEVALE, Alan FACCHINETTI, Luca MAGGIORI, Daniele ROCCHI

Dipartimento di Meccanica, Politecnico di Milano
Via La Masa 1, 20156 Milano, Italy
e-mail marco.carnevale@polimi.it
ph. +39 02 2399 8437 fax +39 02 2399 8492

ABSTRACT

This paper discusses the possibility to adopt Computational Fluid Dynamics (CFD) to assess the influence of aerodynamic forces (aerodynamic uplift) on the mean contact force acting between pantograph and contact wire. The analysis is carried out through experimental tests and CFD simulations, performed both in wind tunnel and on-track scenarios. A method for the computation of the aerodynamic uplift and for the assessment of the contact force unbalance between leading and trailing collector is proposed. It is based on the virtual work principle, and exploits both the numerical forces resulting from CFD analysis and the Jacobian terms obtained from pantograph kinematic analysis. The proposed model only takes into account stationary phenomena; it is fully validated by means of experimental results.

Keywords: computational fluid dynamics, pantograph uplift, wind tunnel, aerodynamic tests.

1. INTRODUCTION

In high speed operation the quality of current collection is significantly affected by aerodynamic forces [1,2], and aerodynamic phenomena need to be taken into account when evaluating the pantograph performances, both in cases of numerical and experimental approaches. One major aerodynamic effect is due to the mean components of the drag and lift forces acting on the moving parts of the pantograph: these forces add their contribution to the uplift force exerted by the pantograph raising mechanism (usually pneumatic), and they are able to change the mean value of the contact force [2,3]. In the following this effect will be indicated as aerodynamic uplift.

When pantographs with two independent collectors are taken into account, aerodynamic steady forces can also generate an unbalance between the mean contact forces of the front and rear collector [1], with a negative outcome on power collection and a non-uniform wear of the two strips.

The unsteady component of the aerodynamic force is due to boundary layer and vortex shedding: possible turbulence in the boundary layer close to the car-body roof is likely to excite the pantograph and affect the performances of the contact force within the frequency range set by the standards for the assessment of current collection quality [1,2]; moreover, vortex shedding, occurring in the wake of pan-head and collectors [1,4], introduces very high-frequency excitation which not only has an impact on aerodynamic noise, but can also worsen the current collection quality, by increasing the sparking level.

Many research works have investigated the possibility to reduce the impact of aerodynamic effects on the quality of current collection. Several of them consider the problems due to average forces [5,6,7,8] and few consider non-stationary phenomena [9], mainly in relation to aero-acoustic issues [4,8]. In practice, for commercial applications, the main countermeasures taken are the compensation of the variability of the mean total contact force and, in some cases, the reduction of the force unbalance on the collectors. Well-established methods to guarantee a proper level of the mean total contact force are the use of aerodynamic spoilers placed on the top of the articulated frame, or the regulation of the uplift force exerted by the air spring at the bottom of the articulated

frame, as a function of train speed and travelling direction [6]. As for the contact force unbalance, the adopted solutions consist again in the use of spoilers placed on each single collector or in a kinematic optimization of the pan-head geometry, aimed at making it as neutral as possible to aerodynamic moment.

Whatever is the adopted solution, the compensation of the aerodynamic forces requires their preliminary evaluation, which is commonly performed by means of on-track measurements according to specific standards (EN50317). Experimental on-track tests are, for the time being, the only way to estimate the aerodynamic uplift in a reliable quantitative way. Wind tunnel experimental tests are indeed a powerful tool, since they allow to assess pantograph aerodynamic behaviour for several test configurations, architectures and design solutions under controlled flow conditions, but their drawback consists in the difficulty of reproducing the actual boundary layer of the train roof, and the turbulence conditions of the wind flow. In [10] the authors point out the importance of the boundary layer reproduction in determining the uplift force in wind tunnel. They propose an effective technique to develop a boundary layer with similar characteristics to the one preliminary measured on the real train, which needs anyway, again, on-track tests to be tuned and validated.

In the last decades, the research concerning the numerical simulation of the dynamic interaction between pantograph and overhead lines has come to its maturity, both regarding the development of suitable techniques for modelling the pantograph, the catenary and the sliding contact, and regarding the sharing of knowledge within the international scientific and technical communities. It has come to an agreement on the main features that have to be developed and taken into account: an international benchmark on the software for the simulation of pantograph-catenary dynamic interaction has been defined in [11], and international specifications set the criteria for software validation (EN50318). On the contrary, computational fluid dynamics (CFD) does not yet represent a mature field for pantograph application and, even if encouraging research results have been obtained in the very last years [12], its accuracy with respect to experimental data has not yet been completely proved [13].

The aim of this work is to study the possibility to assess the influence of aerodynamic forces on pantograph mean contact force by means of CFD modelling, and to identify the pantograph parts that have the largest influence on the uplift force. Wind tunnel experimental tests in smooth flow conditions are exploited to validate the CFD modelling, which is then used to ascertain the aerodynamic behaviour of the same pantograph on a real train, under real flow conditions. In the paper the focus will be drawn on the stationary aerodynamic effects.

CFD results permit the evaluation of the aerodynamic forces acting on each single pantograph component, not trivial to be done experimentally, and therefore allow an accurate assessment of the influence of each component, different geometries, and design solutions on the uplift force. Moreover, the knowledge of drag and lift coefficients of each pantograph component can enhance the numerical simulation of pantograph-catenary dynamic interaction [1,2]: the application of the correct aerodynamic forces on each single component is a relevant feature even when only the stationary force components are taken into account, as for example in the case of pan-head suspension springs having a non-linear behaviour, whose working point can be influenced by the correct application of aerodynamic loads [1].

The paper is organized as follows: in Section 2 the experimental layout for the full scale wind tunnel tests is described. In the following Section 3 the CFD modelling is described, and the numerical results are validated by comparison against experimental aerodynamic global forces and

moments measured in wind tunnel. In Section 4 a procedure for the computation of the total aerodynamic uplift and the force unbalance of the collectors is proposed. It is performed through the virtual work principle and relies on the results of both the CFD simulation and the kinematic analysis of the pantograph. Finally, in Section 5, the results of a simulation of the pantograph installed on the real train are presented, and some conclusions are drawn about the possibility to extend wind tunnel test results, obtained in smooth flow conditions, to the actual on-track application.

2. WIND TUNNEL CHARACTERIZATION

Aerodynamic forces depend on the speed of the incident air flow, which is likely to be lower than the actual train speed due to the development of the boundary layer along the train roof, and on the pantograph orientation, since all the main high speed pantographs show an asymmetrical geometry. In addition, a key role in determining aerodynamic uplift is played by the geometries of pantograph components (e.g.: collector section and articulated frame cylinders section) [1], the working height [14], and, as it will be remarked in the present work, the kinematic links between the vertical displacement of the pan-head and the displacements of the points where aerodynamic forces of each component act [2].

Wind tunnel tests are an helpful tool for a first assessment of the aerodynamic properties of a pantograph, since they allow to test different solutions with known and controlled incoming wind flow. They permit to highlight possible criticalities, and to obtain indications on a newly developed pantograph about the countermeasures needed to achieve the target contact force, before aerodynamic on-track tests are carried out.

Wind tunnel experiments on high speed pantographs are performed at Politecnico di Milano in the high speed, low turbulence chamber, whose main characteristics are reported in Table 1. For the pantograph considered in this work the tests were performed in the closed test section, the blockage ratio being around 3%.

TABLE 1 SHOULD APPEAR HERE

The aim of the experimental campaign was a preliminary evaluation of the aerodynamic quantities (uplift, global drag and lift, lift coefficients and contact force unbalance of the collectors) for different configurations such as wind speed, pantograph orientation and working height, deflection of pan-head suspensions. The pantograph was installed in the test chamber on an aluminium frame linked to the ground through a six-component strain gauge balance placed right below the pantograph centre of mass (Figure 1a), so that all the forces and moments exchanged between the pantograph and the ground could be measured. The aluminium supporting structure and the measuring balance were enclosed below a splitter plate (Figure 1b), so as to cut off the boundary layer developing on the floor and put the pantograph in an uniform flow. The global forces and moments measured by the strain-gauge balance, even if not directly comparable to those affecting the quality of current collection in operating conditions, are of relevant interest in this work since they will be used to validate the numerical results obtained by CFD analysis.

FIGURE 1 SHOULD APPEAR HERE

The contribution of aerodynamic forces to the mean contact force (aerodynamic uplift) was measured by connecting each pantograph collector, through two retaining wires, to a load cell placed at the base of the pantograph fixed frame (Figure 1b): the two cells measured two internal forces, whose sum corresponds to the total contact force which would be exchanged between the collectors and the contact wire. The aerodynamic uplift was computed for each wind speed as the difference between the total force measured during the tests, due to both the air spring force and the aerodynamic uplift, and the force measured in still air, representing the only air spring uplift contribution. This set-up also allowed to measure the contact force unbalance resulting on leading and trailing collector, due to aerodynamic forces on the pan-head: the unbalance was directly computed as the difference between the forces in the two retaining wire, which is null in still air.

Two pantograph orientations, either with the knee upstream or with the knee downstream were considered (see caption of Figure 1a for definition of orientations). Both the orientations were tested at the speeds of 33 m/s, 38 m/s, 44 m/s, 50 m/s and 55 m/s, at two working heights compatible with the actual operating range (i.e. 1.35 m and 1.55 m, measured from the top of the fixed frame to the top of the collectors, as in Figure 1a).

The pan-head of the pantograph adopted in the present work was instrumented with optical load cells, measuring the force acting through the pan-head suspension, and two optical accelerometers placed on each collector. This set-up, according to EN50317, is used during on-track tests to measure the contact force between the collectors and the contact wire.

3. CFD MODELLING AND MODEL VALIDATION

The numerical simulation of pantograph aerodynamic behaviour can be considered tricky due to the following issues: the complex geometry, mainly characterized by cylinders in the articulated frame and bluff bodies in the collector, the high Reynolds number, the high sensitivity of pantograph forces to the boundary layer of the incoming wind flow, which leads to the need of an accurate modelling of the entire train roof. High computational resources are therefore needed, especially when interested in non-stationary phenomena.

The objective of the CFD model developed in this paper is the assessment of the possibility to simulate and reproduce the main aerodynamic effects on the pantograph, adopting modelling criteria of industrial applicability and exploitable in contexts such as design optimization, planning of experimental tests, prediction of the aerodynamic forces acting on the pantograph installed on the car-body roof. The main modelling choices were taken as a trade-off between the accuracy of the achievable results and the costs of the simulations, intended both as hardware resources and computational time needed.

The Reynolds-Averaged Navier-Stokes (RANS) approach was considered of practical interest, since in the case of pantograph applications the main non-stationary phenomena are statistically stable and constant (as in the case of the vortex shedding related to collectors). This approach is based on a temporal filtering of the primitive equations, with the turbulence quantity decomposed in a mean quantity (solved) and a fluctuating quantity (modelled). It allows therefore a sharp decrease of the computational time. Nevertheless, the results sensibly depend on the turbulence model used to close the mathematical problem, and can sometimes be rather inaccurate [15].

In addition to non-stationary simulations, RANS models allow to execute stationary simulations, neglecting the time dependent terms. This choice is considered to be preferable when the effects of aerodynamic forces on the mean contact force are studied, as in the present work. RANS stationary

simulations can indeed be executed within a few hours and therefore be effectively applied to the analysis of several variants and configurations of the same model, as required for pantograph orientations and working heights.

The turbulence model adopted in this work for RANS simulations is the *k-ω SST* [16], which presents a good behaviour in the presence of adverse pressure gradients and flux separation [16], largely occurring on various pantograph components such as cylinder and bluff bodies. Even if the *k-ω SST* model can be used without wall function also within the fine mesh close to the solid surfaces of the pantograph, the use of wall functions was preferred to contain the computational effort and to benefit industrial applicability. The two approaches were initially compared on a single arm of the pantograph, and the differences in results were limited to 10%, with lower force results obtained by using wall functions.

The mesh refinement was carried out through subsequent mesh and simulation steps, as to get the convergence of the solution with a mesh as dense as necessary. The most relevant result of this process is the ascertain of an elevated sensitivity of numerical results to the presence of cell layers close to walls, which need to have high regularity to get accurate results.

The computational domain for simulating the wind tunnel tests is reported in Figure 2, whereas Table 2 reports the main modelling features and boundary conditions adopted.

FIGURE 2 SHOULD APPEAR HERE

TABLE 2 SHOULD APPEAR HERE

The following figures report, in order to validate the CFD model, the comparison between numerical and experimental forces and moments measured in wind tunnel by the strain gauge balance, for the knee-upstream and knee-downstream configurations and the pantograph height of 1.35 m. The attention is focused on drag (Fx), lift (Fz) forces and pitch moment (My), the latter being reduced to the y axis of the coordinate system of Figure 2, placed at the top surface of the pantograph base frame in order to make the results comparable to those of other pantographs.

Figure 3 shows the drag force Fx for knee upstream (a) and knee downstream (b) orientations. The experimental drag forces are equal in the two orientations, and the numerical results are accurate in the considered speed range (from 40 to 55 m/s), with a maximum error equal to 4%.

FIGURE 3 SHOULD APPEAR HERE

Figure 4 reports the total lift force Fz. Also in this case both the knee-upstream (Figure 4a) and knee-downstream (Figure 4b) simulation results fit satisfactory the experimental data (maximum error 25%), showing that the former orientation is subjected to a higher lift force.

FIGURE 4 SHOULD APPEAR HERE

Finally, the pitch moment My is reported in Figure 5. The knee-upstream simulation results (Figure 5a) well fit the experimental data (maximum error 10%), denoting that not only the model is able to reproduce the global forces, but also their distribution on the single components. On the other hand, some discrepancies are obtained for the knee-downstream orientation (Figure 5b), for which the My shows a maximum error of 31%, even if total drag and lift forces are correctly reproduced.

FIGURE 5 SHOULD APPEAR HERE

Both the experimental and numerical moments are lower in the knee-downstream orientation (Figure 5b) than in the knee-upstream case (Figure 5a). Nevertheless, a slight decrease (-10 %) is observed in experimental results from knee-upstream to knee-downstream configuration, a stronger decrease (-30 %) in CFD results.

CFD results allowed to discern the contribution of each pantograph component, represented in Figure 6b, to the total pitch moment. The analysis showed that the main contribution to the total moment is due to the pan-head (e.g.160 Nm at 40 m/s), and does not vary in the two orientations. Negligible contribution is given by the upper arm of the articulated frame, due to the negligible arm (see Figure 8 c and d). Not-negligible contributions are given by the lower arm of the articulated frame and, only for the knee-downstream orientation, by the pantograph fixed frame. The moments generated in the two orientations by these two components vary significantly. In the knee-downstream orientation the lower arm and the fixed frame are immersed in the turbulent wake generated by the air spring placed on the fixed frame, whereas, in the knee-upstream orientation, an unperturbed flow blows over all the component. (This will be discussed in the following and showed in Figure 8 a and b). The simulation of the case in which the turbulent wake interacts with pantograph components seems to be more tricky: an error in the estimation of the pressure distribution, generating an error in the point of application or in the line of action of the forces exerted in this area, is likely to be the reason for the observed error in the My moment in the knee-downstream orientation. According to the aim of the present work, this error can be accepted for two reasons: the forces acting on the fixed frame do not have any role in affecting the contact force; both the fixed frame and the lower arm of the articulated frame do not play a relevant role when the pantograph is installed on the train, being the former shielded by the train-roof recess, the latter blown over by a reduced velocity due to the train roof boundary layer (see Figure 12 and Figure 13).

4. EVALUATION OF THE AERODYNAMIC UPLIFT FORCE

4.1. Total Uplift

CFD software packages allow to calculate the aerodynamic forces and moments acting on each single pantograph component, but do not allow to compute directly the resulting uplift force. The latter can be experimentally measured as the force arising when preventing the vertical displacement of the pantograph head (as in the wind tunnel tests described in section 2), but is not easily reproducible by CFD model, in which the pantograph is regarded as a rigid body and the kinematic links are not taken into account. From a mechanical point of view the aerodynamic uplift is the Lagrangian component of all the aerodynamic forces over the pan-head displacement: its numerical estimation can therefore be obtained by the application of the virtual work principle (equation 1), in which the virtual work done by all the drag (Fx_i) and lift (Fz_i) forces acting on each i-th component is equal to the virtual work of the aerodynamic uplift F_{uplift}. The points of application of the CFD forces on each pantograph part are chosen as to have null moments, so that only forces are considered in the virtual work principle.

$$\sum_i Fx_i \delta x_i + \sum_i Fz_i \delta z_i = F_{Uplift} \delta z_h \quad (1)$$

The Jacobian terms, relating the vertical displacement of the pan-head (δz_h) to the horizontal (δx_i) and vertical (δz_i) displacements of the points of application of the aerodynamic forces, have a great role in determining the resulting aerodynamic uplift. They can be calculated by considering the pantograph as a single degree of freedom system, based on the four bar linkage constituting the articulated frame, and neglecting the deflection of the pan-head suspension. Figure 6 reports a scheme of the kinematic model (Figure 6a) and a scheme of all the forces considered in the uplift computation (Figure 6b).

FIGURE 6 SHOULD APPEAR HERE

The estimation of the aerodynamic uplift obtained by the method described above can be considered very satisfying: Figure 7 compares numerical and experimental wind tunnel results for both the pantograph orientations, i.e. knee-upstream (Figure 7a) and knee-downstream (Figure 7b). The model is able to correctly reproduce the uplift corresponding to different test conditions.

FIGURE 7 SHOULD APPEAR HERE

A positive uplift, which would increase the mean contact force, is observed in the former case, a negative one in the latter. Uplift forces are not symmetrical, with the positive values higher than the corresponding negative values (e.g. 48 N vs. -15 N for the speed of 55 m/s). Moreover, in the case of upstream knee (Figure 7a) the uplift forces are very relevant: the experimental tests, carried out up to 55 m/s, show a trend that leads to the prediction of an aerodynamic uplift equal to 104 N at the speed of 83 m/s (300 km/h). This could be critical for the considered pantograph, since the only aerodynamic force contribution is close to the maximum mean contact force borne by specifications (e.g. 157 N at 300 km/h according to the Technical Specification for Interoperability, TSI, 25 kV). Therefore, when installing the pantograph on a train car-body roof, the need to use shields or shrouds should be considered.

The reason of the asymmetry of the uplift forces obtained in the two pantograph orientations can be investigated by analysing the numerical velocity fields and the forces acting on each single pantograph components, reported in Figure **8** for the speed of 40 m/s.

FIGURE 8 SHOULD APPEAR HERE

The main differences in the wind flows (Figure 8a and Figure 8b) can be observed in the stream acting on the lower arm of the articulated frame: in the knee-upstream case (Figure 8a) an unperturbed flow impacts on the pantograph articulated frame, whereas in the knee-downstream case (Figure 8b) a shielding effect is carried out by the air-spring (highlighted with a circle in the figure), which generates some turbulence in the flow interacting with the lower arm. This shielding effect can be regarded as the reason of the asymmetry of the uplift forces corresponding to the two pantograph orientations, already pointed out in Figure 7. This is clearly visible by looking at the forces exerted on the pantograph parts, highlighted in Figure 8c and Figure 8d: when comparing the knee-upstream (Figure 8c) and the knee-downstream configurations (Figure 8d), the forces on each component show similar intensity and opposite direction, exception made for the force on the bottom arm of the articulated frame: this differs significantly in intensity and also in the action line, being affected by the air-spring shielding in the case of knee-downstream.

These results lead to the conclusion that the CFD model is able to catch the main peculiarities occurring in the pantograph behaviour.

In addition to the estimation of the total uplift, the joint application of CFD and virtual work principle allows the achievement of another important outcome: the assessment of the contribution of each single pantograph element to the total uplift. It is worth recalling that, due to the x-direction component of each virtual displacement, also the drag forces can have a remarkable impact on the uplift force (see equation 1). To deepen this point, Figure 9a reports the results of the kinematic analysis of the pantograph, according to the model of Figure 6a.

FIGURE 9 SHOULD APPEAR HERE

Different positions are represented, corresponding to different pantograph heights. As an example the attention is focused on the positions assumed by the pan-head (squares), indicated in Figure 9a with C, C', C'' and C'''. The pan-head trajectory corresponding to a complete pantograph raising is reported in Figure 9b: at the working height analysed in this work (i.e. 1.35 m), a significant component of horizontal displacement is observed, meaning that the virtual work done by the drag force acting on the pan-head is rather relevant, and, as a consequence, the drag force has a relevant contribution to the total uplift.

The bar diagram in Figure 10 reports, for each i-th pantograph component named in Figure 6b and indicated in the x-label, the contribution to the global uplift due to the drag force (white bars), and due to the lift force (gray bars), representing respectively the terms $Fx_i \frac{\delta x_i}{\delta z_h}$ and $Fz_i \frac{\delta z_i}{\delta z_h}$ in the summations of equation 1. In the same Figure 10 the black bars represent the contribution due to the total force (sum of drag and lift components).

FIGURE 10 SHOULD APPEAR HERE

Some main remarks can be done. Due to the kinematic links, the drag forces tend to open the pantograph and to increase the uplift force in the case of knee-upstream orientation (Figure 10a), and they show the opposite behaviour for the knee-downstream orientations (Figure 10b), tending to close the pantograph and giving a negative contribution to the uplift force.

In the case of the knee-upstream orientation (Figure 10a), in which the pantograph is blown over by unperturbed flow, the parts of the pantograph which mainly affect the aerodynamic uplift force are the lower arm and the upper arms of the articulated frame, giving opposite contributions: the bottom arm shows a positive uplift, whereas the upper arms a negative uplift. The latter is the result of a negative contribution due to the lift force, and a positive contribution due to the drag force. On the contrary, in the knee-downstream configuration (Figure 10b), the signs of lower and upper arm contributions are inverted, and the effect of the lower arm is less relevant due to the shielding effect generated by the air spring. In this case, the dominant role is played by the upper arms and the pan-head.

The force acting on the pantograph head is essentially drag force, with a slight down-lift contribution clearly visible also in Figure 8c and Figure 8d. The drag component has a relevant impact on the uplift force, due to the high Jacobian term $\frac{\partial x_h}{\partial z_h}$ (indicating the horizontal displacement of the pan-head δx_h over a vertical displacement δz_h, see Figure 9b). This is an aspect which should be carefully taken into account when designing a new pantograph, and minimised by means of proper kinematic optimization.

4.2. Contact force unbalance on leading and trailing collectors

When evaluating the quality of current collection, a correct value of the total contact force could not be sufficient to guarantee good performances: contact force unbalance between leading and trailing collectors needs also to be monitored, since it can lead to excessive force on one collector and contact losses on the other one, with consequent non uniform current flow through the pantograph components. Contact force unbalance is mainly generated by the aerodynamic forces acting on the pan-head, which are equilibrated by the contact forces on each collector.

Using the same approach adopted in paragraph 4.1 for the numerical evaluation of the aerodynamic uplift, the contact force unbalance occurring on pantograph collectors can successfully be assessed, relying on CFD results. The virtual work of all the aerodynamic forces acting on the pan-head, obtained from CFD, has to equal the virtual work of the contact forces acting on the collectors, unknown in CFD computation. To this purpose, the kinematics of the pan-head is analysed by considering also its degree/s of freedom relative to the pantograph frame, properly chosen on the basis of the pan-head architecture.

It is worth pointing out that, if on the one hand the kinematic analysis of the pantograph articulated frame described in paragraph 4.1 is applicable to all the modern pantograph, on the other hand the pan-head kinematics can be rather different for different kinds of pantograph, since several architectures are used nowadays. Two examples among others are given: the pantograph adopted in [1] shows independent collectors and no direct force transfer between leading and trailing bows. In this case the contact force unbalance is related to the suspension geometry which couples the effect of the horizontal and vertical forces on each collector. In the pan-head architecture used in [17], having a pitch degree of freedom which allows a direct load transfer between leading and trailing collector, the contact force unbalance is mainly due to the need for leading and trailing contact forces to balance the aerodynamic moment.

Figure 11 reports the wind tunnel results obtained for the case under analysis, in which the whole pan-head can rotate with respect to the articulated frame about its pitch axis. In particular, Figure 11a refers to the knee-upstream configuration, Figure 11b to knee-downstream one. The figures report the force variations, with respect to the still air condition, measured at different wind speeds by the load cells at the end of the retaining wires of each collector. The sum of the forces acting on leading and trailing collector is equal to the total uplift already shown in Figure 7, whereas their difference represents the contact force unbalance.

Regardless the pantograph orientation, the highest contact force is observed on the trailing collector, meaning that, for the analysed pan-head geometry, the centre of pressure of the aerodynamic forces is always placed below the centre of rotation of the pitch degree of freedom. CFD results are able to identify this fact, and allow to properly estimate the contact force unbalance, which is slightly overestimated in the knee-upstream configuration, and underestimated for the knee-downstream case.

FIGURE 11 SHOULD APPEAR HERE

5. EXTENSION OF THE MODEL TO THE FULL TRAIN AND VALIDATION

The instrumented pantograph tested in wind tunnel was also used for aerodynamic track tests on a full-scale train, in which the uplift force was measured with the method described in section 2, exploiting one retaining wire for each collector and measuring the corresponding force by means of load cells placed on the pantograph fixed frame. During the tests, the pantograph was hold at the distance of 70 mm from the contact wire, so as to avoid any dynamic interaction with the catenary and to measure only the aerodynamic forces according to EN50317. This distance corresponds to the working height of 1.41 m, which is in between the two heights tested in wind tunnel (i.e. 1.35 m and 1.58 m), for which no height dependence was obtained. In the train used for on-track tests, two 25 kV pantographs are placed on two contiguous coaches in the middle of the train, and each pantograph is placed in a recess area designed with the aim of shielding it as much as possible from air. Since the measuring pantograph was not in contact with the contact wire, the other pantograph was used to supply the traction power and to launch the train to the test speed. For the case of knee-downstream configuration the traction pantograph was upstream the measuring one, affecting the incoming flow. In this case, the uplift results were recorded with the train unpowered, during the coasting, with the upwind pantograph closed and with only the instrumented pantograph raised.

The aim of these tests was to measure the uplift force in the real operating conditions, where the incoming flow on the pantograph is altered by the particular train roof geometry and by the pantograph recess turbulence [13, 18], to understand how wind tunnel results can be extended to the full scale train [10]. To this purpose, the complete train was also simulated, using the same CFD RANS model (k-ω SST), the same boundary conditions and the same mesh of the instrumented pantograph validated by wind tunnel tests. A dense mesh was used to describe the development of the boundary layer along the train roof preceding and immediately following the measuring pantograph (also including the non-instrumented lowered pantograph), whereas a coarser mesh was used for the body side, the vehicle floor and entirely for the rear coaches. The cell number of the complete model was around 40 millions. This value, if compared to the 20 million cells used for the wind tunnel simulation, points out that an accurate mesh of the pantograph requires about a half of the cell number of the total train simulation.

Figure 12 reports the comparison of numerical and experimental aerodynamic uplift results up to the speed of 300 km/h. In the present work only the results corresponding to out-of-tunnel line sections are taken into account. The experimental data, obtained as the average uplift force corresponding to 1 second intervals, are reported by star markers, whereas the filled squares represent the results of CFD simulations.

FIGURE 12 SHOULD APPEAR HERE

A good fitting of the experimental data is obtained by means of CFD analysis. Moreover, the fact that the pantograph installed on the train shows a negative uplift for both the knee-upstream and knee-downstream orientations, which is the most evident difference with respect to wind tunnel results, is clearly pointed out by numerical simulations.

The comparison between full train and wind tunnel uplift results shows very different results for the knee-upstream case (Figure 12a vs. Figure 7a). This is due to the presence of the recess and of the cover installed on the train roof immediately before the pantograph (see the following Figure 13 for the train lay-out), which generate a shielding effect which is not present in the wind tunnel.

As for the knee-downstream pantograph, the train results are almost coincident with the wind tunnel results of the instrumented pantograph (Figure 12b vs. Figure 7b), with similar uplift forces obtained at the same nominal speeds. For this orientation the shielding effect created by the recess and the cover on the train does not change the results very much, since it only overlaps its effect to the shielding created by the air spring, already described (see Figure 8) for the wind tunnel pantograph. The similarity of the overall uplift results should not lead to the assumption that the results of wind tunnel tests can be directly extended to the evaluation of the uplift of the pantograph installed on a real train. From an aerodynamic point of view the two cases are indeed very different: due to the boundary layer developed along the train roof, the wind profile acting on the pantograph is very different from the one corresponding to the wind tunnel case, as much as the role of the single pantograph components in determining the total aerodynamic uplift. This fact will be shown in the following.

Figure 13 reports the longitudinal velocity field U related to the knee-downstream configuration at the simulation speed of 200 km/h (55 m/s), this speed being selected in order to compare the train results with the maximum velocity tested in wind tunnel.

FIGURE 13 SHOULD APPEAR HERE

Figure 13a reports the velocity field along the whole train. In addition to the two already mentioned 25 kV pantographs used during the tests, another couple of pantographs is installed on the train respectively in two recesses at the second and penultimate coaches. The velocity field (Figure 12a) shows a flow separation at the front recess, where the flow is deviated upwards. At the considered speed, the boundary layer has an extension of around 0.4 m before the first recess and gets 0.8 m immediately after it (dashed lines 1 and 2 in Figure 13a). The height keeps on increasing along the train roof and reaches 1.8 m immediately before the instrumented pantograph (dashed line 3 in Figure 13a), and 2.25 m before the last recess in the rear coaches (dashed line 4).

The instrumented pantograph (enlargement of Figure 13b) is therefore entirely placed within the boundary layer, and the maximum velocity of the wind acting on it is lower than the train speed (49 vs. 55 m/s). Each part is affected by an incoming wind profile rather different from the wind tunnel one.

Figure 14a reports the comparison of the numerical non-dimensional wind profiles $\left(\frac{U}{U_\infty}\right)$ detected 0.5 m before the measuring pantograph, for the wind tunnel (solid line) and the train case (dashed line). As for the former, the incoming flow speed is almost constant and equal to the nominal test speed U_∞, and the boundary layer height is contained to some centimetres. On the contrary, for the train case, the velocity of the wind acting on the upper arm of the articulated frame and on the pan-head is around 0.8 times the train speed U_∞. In correspondence to the lower arm of the articulated frame, the non-dimensional speed decreases sharply down to the height of the cover installed on the car-body roof (0.23 m).

FIGURE 14 SHOULD APPEAR HERE

Figure 14b compares the CFD results of train and wind tunnel simulations in terms of contribution of each pantograph component to the total uplift. The data are presented in the figure as the uplift

force exerted by each component per unit of kinetic energy of the incoming wind $\left(c_u S = \frac{F_u}{\frac{1}{2}\rho U_\infty^2}\right)$, with the uplift forces F_u calculated by means of the procedure described in section 4.1, and the kinetic energy corresponding to the nominal speed U_∞ (ρ=1.22 kg/m^3).

Due to the reduced velocity in the boundary layer, the component coefficients of the pantograph installed on the train are generally lower than the wind tunnel ones. As an example, the velocity of the wind acting on the pan-head in the train case is 0.88 times the corresponding wind tunnel speed; as a consequence of this, the uplift coefficient $c_u S$ of the pan-head is 0.85 times the value obtained in wind tunnel (i.e.: $c_u S = -0.0134$ in the train case vs. $c_u S = -0.0158$ in the wind tunnel case). Moreover, the weight of each single component is rather different in the two cases, depending on the development of the boundary layer along the pantograph. In wind tunnel the coefficient $c_u S$ of the lower arm of the articulated frame is nearly half the pan-head coefficient, whereas for the real train, as an effect of the different velocities acting on the two components, the ratio between the lower arm and the pan-head coefficients decreases to 0.31. Besides, the rear arm is negligible in the train case, due to the very low speed of the wind acting on it.

These remarks point out that the wind profile has a relevant role in determining which of the pantograph components are noteworthy in affecting the uplift force.

As a conclusion of this section, Figure 15 shows how, for the train case, the uplift force is distributed on each single collector (contact force unbalance). The results measured in the retaining wires during on-track experimental tests are compared to the ones evaluated numerically on the basis of the method described in paragraph 4.2. As already pointed out for the wind tunnel case (see Figure 11), the contact force on the trailing collector is higher than the one acting on the leading collector for both pantograph orientations (knee-upstream in Figure 15a, knee-downstream in Figure 15b). The numerical results fit very well the experimental ones, leading, as in the case of wind tunnel test, to a correct evaluation of the contact force unbalance.

FIGURE 15 SHOULD APPEAR HERE

6. CONCLUSIONS

The paper demonstrated the possibility to assess, by means of CFD, the influence of aerodynamic forces on the pantograph mean contact force. The analysis was carried out by comparing CFD results with experimental wind tunnel and on-track results. Stationary simulations are adequate and even preferable, in order to contain the computational effort and the hardware required, which is not small advantage for industrial applications.

CFD simulations allowed, together with the kinematical analysis of the pantograph and the application of the virtual work principle, the estimation of the aerodynamic uplift force and the assessment of the role played by each component. It was shown that not only the component geometries, but also a correct design of pantograph kinematics is very relevant in order to contain the perturbation of the mean contact force due to aerodynamic forces. The virtual work principle was also adopted for the estimation of the contact force unbalance on the collectors, due to aerodynamic forces.

After being validated by means of wind tunnel test results, the CFD model was exploited to simulate the real train scenario, and validated against experimental on-track results. Fluid dynamic simulations supplied relevant information on the incoming wind flow and on the influence of the

car-body roof geometry, allowing the ascertainment of the differences between wind tunnel and on-track pantograph forces, mainly due to the different boundary layers.
The possibility to achieve the above results by means of CFD allows to shift from a test stage to a design stage part of the evaluation of pantograph aerodynamic properties, and the assessment of different design solutions. This is an important outcome, since track tests are quite expensive, and wind tunnel tests do not always permit the straightforward evaluation of the actual uplift forces, due to the need to reproduce the mean vertical wind profile corresponding to the boundary layer of the real train.

7. ACKNOWLEDGEMENTS

The authors would like to thank the companies Contact s.r.l., Schunk GmbH and Bombardier Transportation for giving the opportunity to carry out the experimental tests.

8. REFERENCES

[1] BOCCIOLONE, M., RESTA, F., ROCCHI, D., TOSI, A. and COLLINA, A., 2006. Pantograph aerodynamic effects on the pantograph-catenary interaction. Vehicle System Dynamics, 44, pp. 560-570.

[2] POMBO, J., AMBROSIO, J., PEREIRA, M., RAUTER, F., COLLINA, A. and FACCHINETTI, A., 2009. Influence of the aerodynamic forces on the pantograph-catenary system for high-speed trains. Vehicle System Dynamics, 47(11), pp. 1327-1347.

[3] LEE, Y., PAIK, J., KWAK, M., YOO, J., KIM, K.H., LEE, D. and KWON, H., 2012. Analysis and comparison of experimental results both of wind tunnel test and running test for HEMU-400X pantograph, 2012 Joint Rail Conference, JRC 2012, April 17, 2012 - April 19, 2012 2012, American Society of Mechanical Engineers, pp. 169-172.

[4] IKEDA, M. and MITSUMOJI, T., 2009. Numerical estimation of aerodynamic interference between panhead and articulated frame. Quarterly Report of RTRI (Railway Technical Research Institute) (Japan), 50(4), pp. 227-232.

[5] SUZUKI, M., IKEDA, M. and KOYAMA, T., 2007. Flow control on pantograph with air intake and outlet. Quarterly Report of RTRI (Railway Technical Research Institute) (Japan), 48(4), pp. 236-239.

[6] BUCCA, G., CARNEVALE, M., COLLINA, A., FACCHINETTI, A., DRUGGE, L., JONSSON, P. and STICHEL, S., 2012. Adoption of different pantographs preloads to improve multiple collection and speed up existing lines. Vehicle System Dynamics, 50, pp. 403-418.

[7] Ikeda, M.; Manabe, K. Development of low noise pantograph with passive lift suppression mechanism of pan-head. Quarterly Report of RTRI (Railway Technical Research Institute) (Japan), 2000, 41, 4, 177-181

[8] LEE, Y., RHO, J., KWAK, M., LEE, J., KIM, K. and LEE, D., 2009. Aerodynamic characteristics of high speed train pantograph with the optimized panhead shape, 7th IASME / WSEAS International Conference on Fluid Mechanics and Aerodynamics, FMA '09, August 20, 2009 - August 22, 2009 2009, World Scientific and Engineering Academy and Society, pp. 84-88.

[9] TUISSI, A., BASSANI, P., CASATI, R., BOCCIOLONE M., COLLINA, A, CARNEVALE M., LO CONTE A., PREVITALI B., 2009. Application of SMA composites in the collectors of the railway pantograph for the Italian high-speed train. Journal of Materials Engineering and Performance, 18, 5-6, 612-619.

[10] TAKAISHI, T. and IKEDA, M., 2012. Experimental method for wind tunnel tests to simulate turbulent flow on the roof of high-speed trains. Quarterly Report of RTRI (Railway Technical Research Institute), 53(3), pp. 167-172.

[11] BRUNI S., & Al. The results of the pantograph–catenary interaction benchmark. Vehicle System Dynamics, 53 (3), pp. 412-435.

[12] LEE, J., CHO, W. Prediction of low speed-aerodynamic load and aeroacoustic noise around simplified panhead section model. Proceedings of the Institution of Mechanical Engineers, Part F: Journal of Rail and Rapid Transit, Vol. 222, pp. 423–431.

[13] YAO, S., GUO, D. and YANG, G. The influence of pantograph aerodynamic characteristics caused by its shroud, 1st International Workshop on High-Speed and Intercity Railways, IWHIR 2011, July 19, 2011 - July 22, 2011 2012, Springer Verlag, pp. 41-52.

[14] LV, Q., LI, R., WANG, S., ZHOU, N. and ZHANG, W., 2014. The Effect of the Working Height of Pantographs on Pantograph-Catenary Dynamic Performance. Proceedings of the Second International Conference on Railway Technology: Research, Development and Maintenance, (paper 146), pp. 1-11.

[15] CATALANO, P., WANG, M., IACCARINO, G. MOIN, P. Numerical simulation of the flow around a circular cylinder at high Reynolds numbers. International Journal of Heat and Fluid Flow 24 (2003) pp. 463–469.

[16]MENTER, F., July 6-9, 1993. Zonal Two Equation k-w Turbulence Models For Aerodynamic Flows, 1993/07/06 July 6-9, 1993, pp. 1-21.

[17]LEE, Y., RHO, J., KIM, K.H., LEE, D. and KWON, H., 2015. Experimental Studies of Aerodynamic Characteristics on High-Speed Train Pantograph. Proceedings of the Institution of Mechanical Engineers, Part F: Journal of Rail and Rapid Transit, Vol. 229(2) 136–149.

[18]NOGER, C., PATRAT, J.C., PEUBE, J. and PEUBE, J.L., 2000. Aeroacoustical study of the TGV pantograph recess. Journal of Sound and Vibration, 231(3), pp. 563-575.

Table Captions

Table 1: Main characteristics of the high speed, low turbulence chamber adopted.

Table 2: Main modelling features and boundary conditions adopted for the CFD simulation (pressure p and velocity U).

Figure Captions

Figure 1: Pantograph layout in wind tunnel. (a) Scheme of the strain-gauge balance and supporting structure. According to the wind arrow, the scheme represents the knee-downstream configuration. (b) Test section layout, with the pantograph held by retaining wires.

Figure 2: Computational domain for simulating the wind tunnel tests.

Figure 3: Drag force Fx. Numerical and experimental results. (a) Knee-upstream. (b) Knee-downstream.

Figure 4: Lift force Fz. Numerical and experimental results. (a) Knee-upstream. (b) Knee-downstream.

Figure 5: Pitch moment My. Numerical and experimental results. (a) Knee-upstream. (b) Knee-downstream.

Figure 6: Pantograph kinematic scheme. (a) Four bar linkage. (b) Forces taken into account for the uplift computation.

Figure 7: Pantograph aerodynamic uplift: comparison of numerical and experimental results. (a) knee-upstream pantograph, height 1.35 m. (b) knee-downstream pantograph, height 1.35 m.

Figure 8: CFD results, instrumented pantograph, speed 40 m/s, pantograph height 1.35 m. (a) Knee-upstream, velocity field. (b) Knee downstream, velocity field. (c) Knee-upstream CFD forces. (d) Knee-downstream, CFD forces.

Figure 9: (a) Example of kinematic analysis of the pantograph. (b) Pan-head trajectory.

Figure 10: Analysis of the contributes of each pantograph component to the total uplift force. Instrumented pantograph, height 1.35 m, speed 40 m/s. (a) Knee-upstream. (b) Knee downstream.

Figure 11: Collector aerodynamic uplift: comparison of numerical and experimental results. (a) Knee-upstream. (b) Knee-downstream.

Figure 12: Numerical vs. experimental uplift results of the pantograph installed on a real train. (a) Knee-upstream. (b) Knee-downstream.

Figure 13: Train simulation results, knee-downstream, speed 200 km/h. (a) Longitudinal velocity field along the whole train. (b) Enlargement of the zone close to the pantograph under test.

Figure 14: Comparison of train and wind tunnel results. (a) Wind profiles acting on the pantograph. (b) Uplift coefficients of instrumented pantograph components. Knee downstream.

Figure 15: Collector aerodynamic uplift: comparison of numerical and experimental on-track results. (a) Knee-upstream. (b) Knee-downstream.

High speed, low turbulence test section		
Section area (wxh)	[m]	4x4
Maximum speed	[m/s]	55
Turbulence Intensity I_u	[%]	0.2

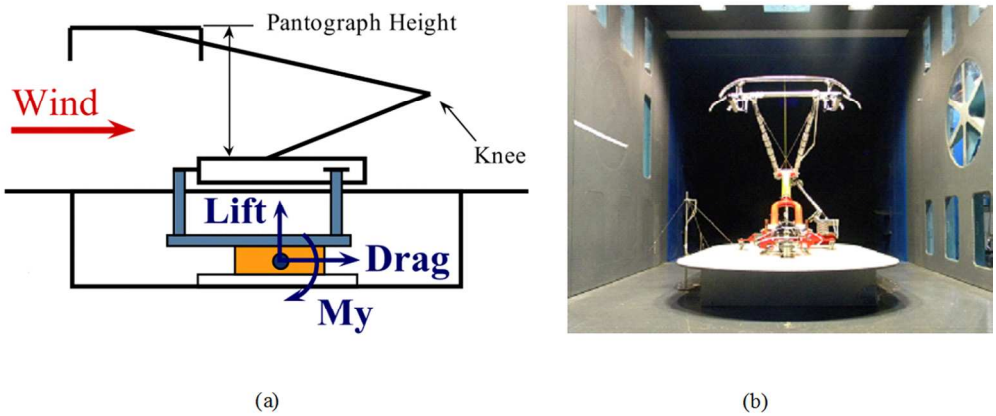

Figure 1: Pantograph layout in wind tunnel. (a) Scheme of the strain-gauge balance and supporting structure. According to the wind arrow, the scheme represents the knee-downstream configuration. (b) Test section layout, with the pantograph held by retaining wires.
101x42mm (300 x 300 DPI)

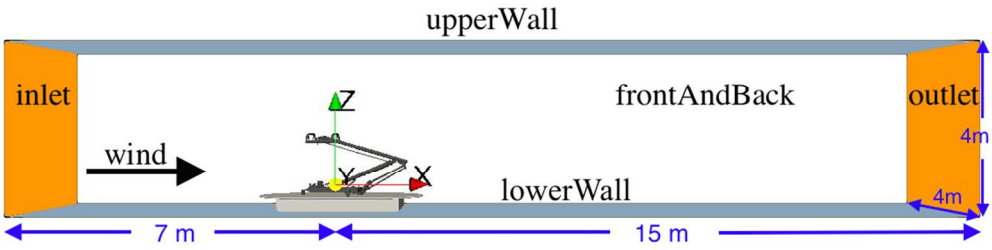

Figure 2: Computational domain for simulating the wind tunnel tests.
96x24mm (300 x 300 DPI)

Patch Name	p	U
Inlet	$\nabla p = 0$	U_∞
Outlet	0	$\nabla U = 0$
Lower wall	$\nabla p = 0$	0
Upper wall	Symmetry plane	
Front and Back	Symmetry plane	
Pantograph surfaces	$\nabla p = 0$	0
Board	$\nabla p = 0$	0

Analysis approach	RANS
Time-dependency	Stationary
Turbulence model	k-ω SST
Discretization scheme	Upwind

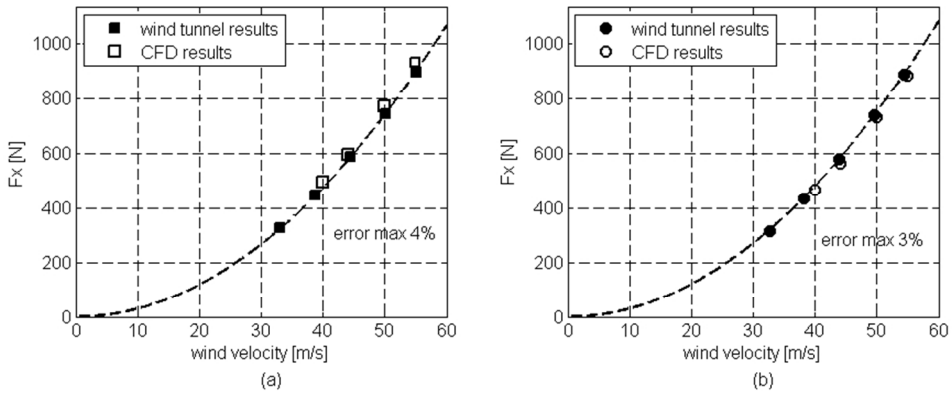

Figure 3: Drag force Fx. Numerical and experimental results. (a) Knee-upstream. (b) Knee-downstream. 77x32mm (300 x 300 DPI)

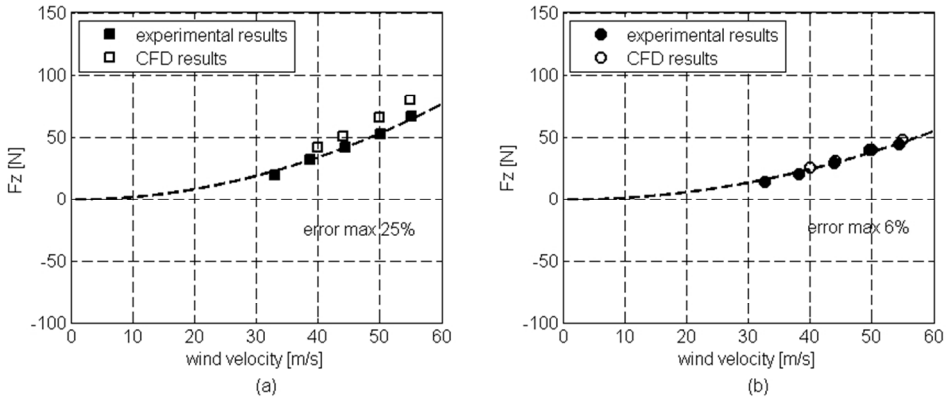

Figure 4: Lift force Fz. Numerical and experimental results. (a) Knee-upstream. (b) Knee-downstream. 77x32mm (300 x 300 DPI)

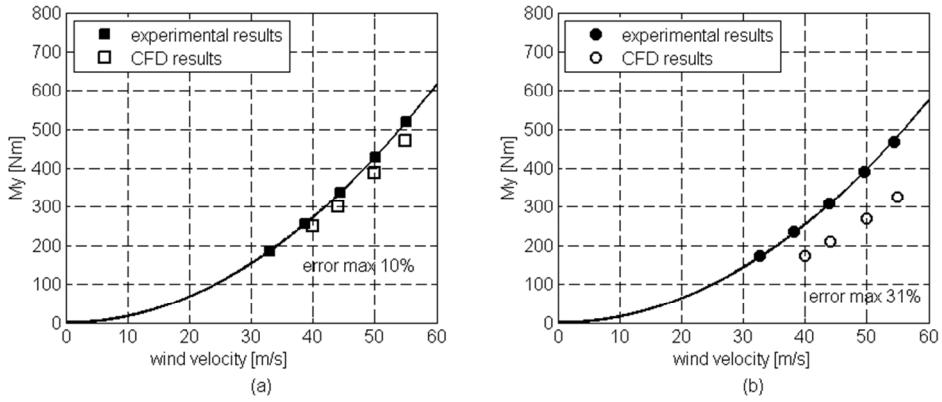

Figure 5: Pitch moment My. Numerical and experimental results. (a) Knee-upstream. (b) Knee-downstream. 77x32mm (300 x 300 DPI)

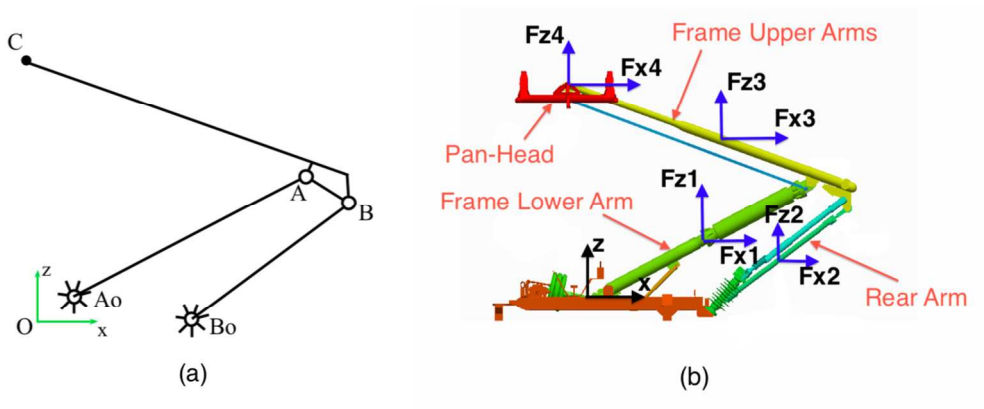

Figure 6: Pantograph kinematic scheme. (a) Four bar linkage. (b) Forces taken into account for the uplift computation.
125x50mm (300 x 300 DPI)

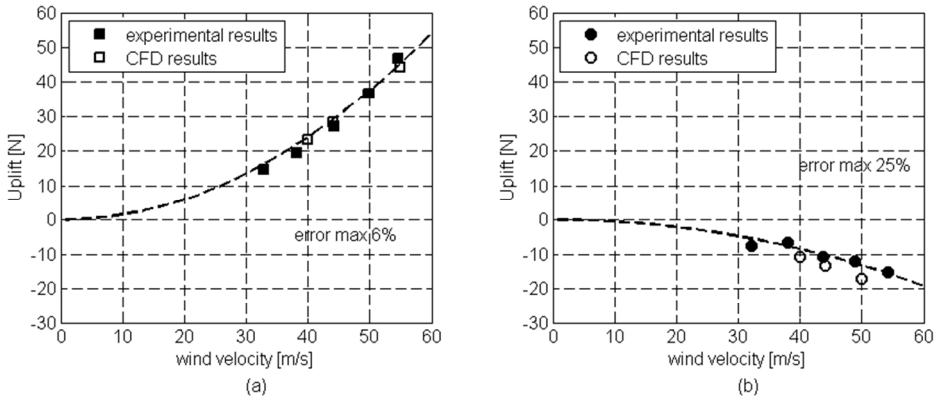

Figure 7: Pantograph aerodynamic uplift: comparison of numerical and experimental results. (a) knee-upstream pantograph, height 1.35 m. (b) knee-downstream pantograph, height 1.35 m.
77x32mm (300 x 300 DPI)

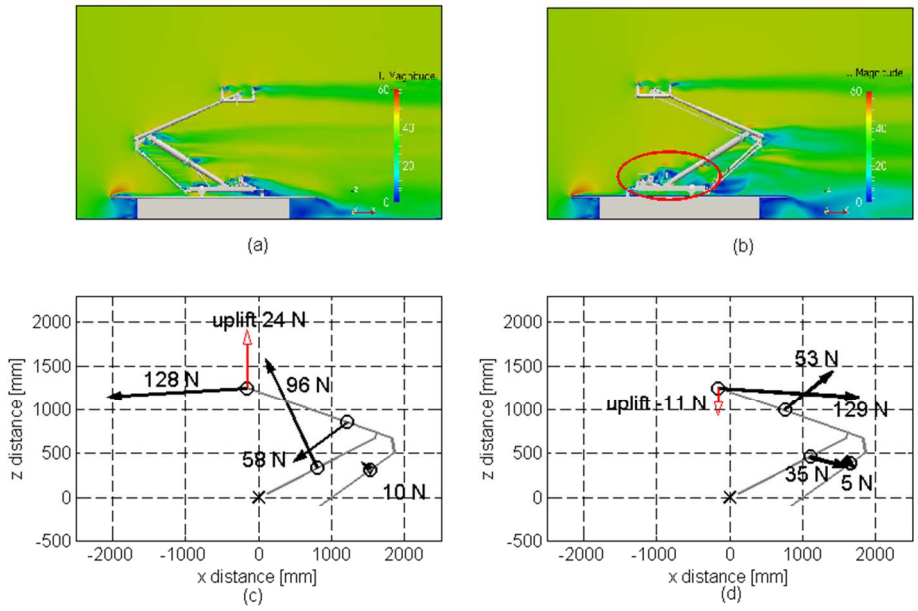

Figure 8: CFD results, instrumented pantograph, speed 40 m/s, pantograph height 1.35 m. (a) Knee-upstream, velocity field. (b) Knee downstream, velocity field. (c) Knee-upstream CFD forces. (d) Knee-downstream, CFD forces.
77x48mm (300 x 300 DPI)

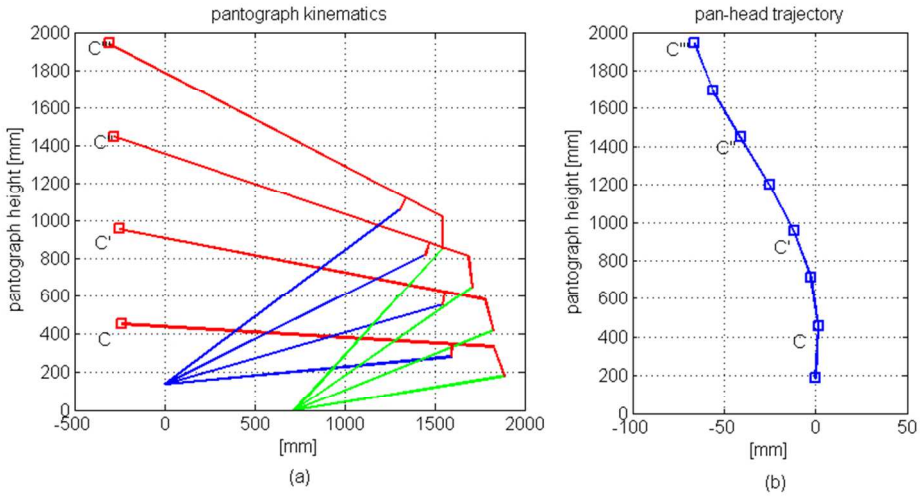

Figure 9: (a) Example of kinematic analysis of the pantograph. (b) Pan-head trajectory.
76x39mm (300 x 300 DPI)

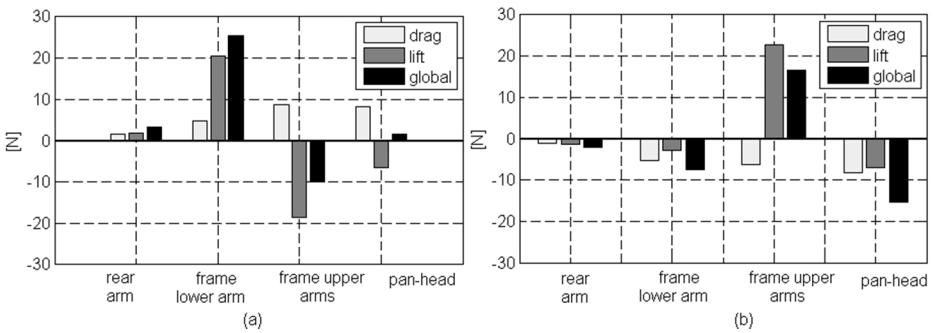

Figure 10: Analysis of the contributes of each pantograph component to the total uplift force. Instrumented pantograph, height 1.35 m, speed 40 m/s. (a) Knee-upstream. (b) Knee downstream.
83x27mm (300 x 300 DPI)

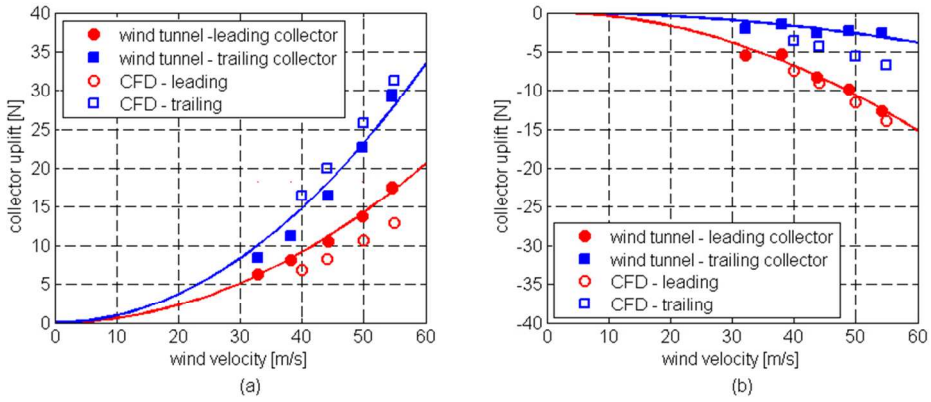

Figure 11: Collector aerodynamic uplift: comparison of numerical and experimental results. (a) Knee-upstream. (b) Knee-downstream.
77x32mm (300 x 300 DPI)

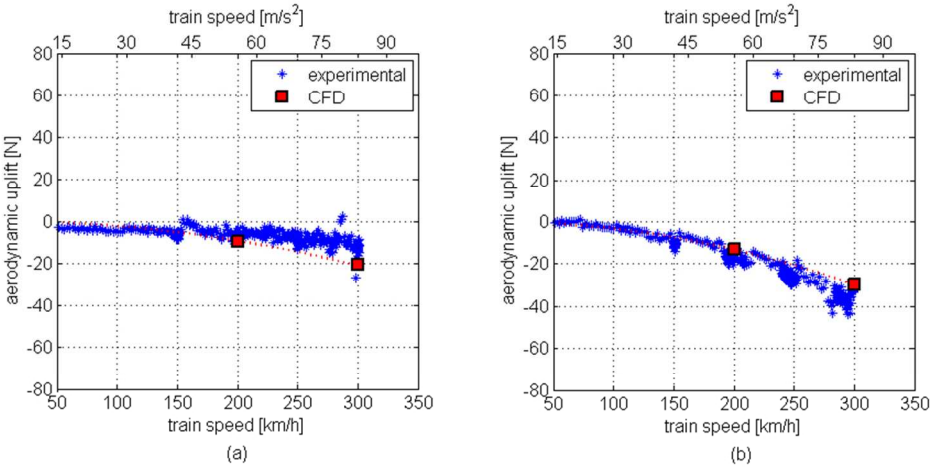

Figure 12: Numerical vs. experimental uplift results of the pantograph installed on a real train. (a) Knee-upstream. (b) Knee-downstream.

77x36mm (300 x 300 DPI)

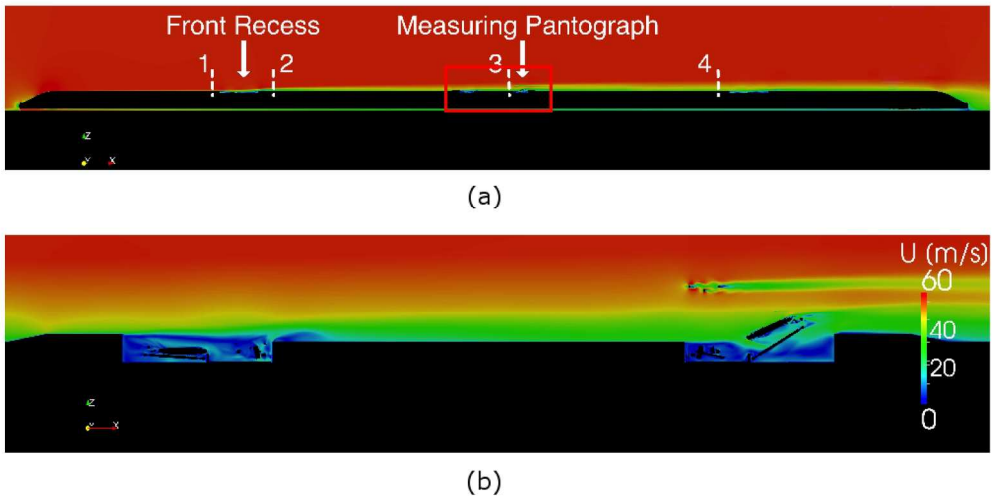

Figure 13: Train simulation results, knee-downstream, speed 200 km/h. (a) Longitudinal velocity field along the whole train. (b) Enlargement of the zone close to the pantograph under test.
189x99mm (300 x 300 DPI)

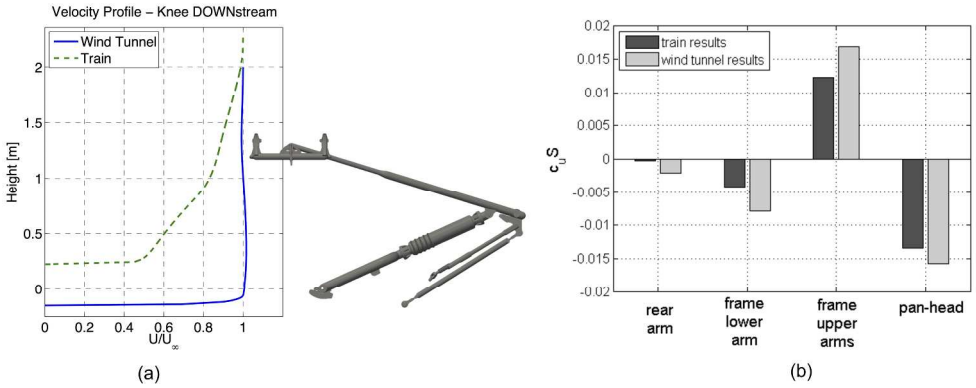

Figure 14: Comparison of train and wind tunnel results. (a) Wind profiles acting on the pantograph. (b) Uplift coefficients of instrumented pantograph components. Knee downstream.
283x109mm (300 x 300 DPI)

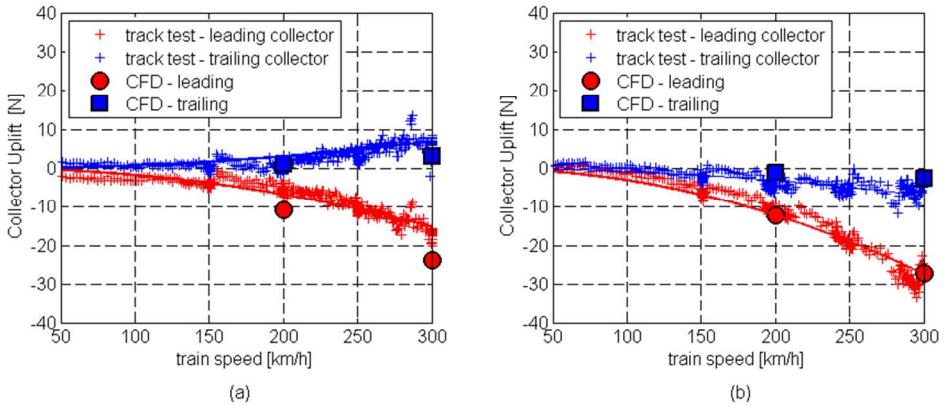

Figure 15: Collector aerodynamic uplift: comparison of numerical and experimental on-track results. (a) Knee-upstream. (b) Knee-downstream.
77x32mm (300 x 300 DPI)